Proposal of New Tracer Concentration Model in Lung PCT Study
Comparison with Commonly Used Gamma-variate Model

Maciej Browarczyk[1], Renata Kalicka[1] and Seweryn Lipiński[2]

[1]*Department of Biomedical Engineering, Gdańsk University of Technology, Narutowicza 11/12 Street, Gdańsk, Poland*
[2]*Department of Electrical Engineering, Power Engineering, Electronics and Automation,*
University of Warmia and Mazury, Olsztyn, Poland

Keywords: Modelling, pCT, Gamma-Variate, Gauss, Rayleigh.

Abstract: Perfusion computed tomography (pCT) is one of the methods that enable non-invasive imaging of the hemodynamics of organs and tissues. On the basis of pCT measurements, perfusion parameters such as blood flow (*BF*), blood volume (*BV*), mean transit time (*MTT*) and permeability surface (*PS*) are calculated and then used for quantitative evaluation of the tissue condition. To calculate perfusion parameters it is necessary to approximate concentration-time curves using regression function. In this paper we compared three regression functions: first commonly used gamma-variate function, second and third Gauss and Rayleigh functions, not previously used for this purpose. The Gauss function showed clear advantage over the others when considering results of simulated data analysis. Actual measurements analysis confirmed conclusions from simulated data analysis. It was showed that contrary to widely accepted belief, the differences between rising and falling edge slope angles of concentration-time curves are inconsiderable. For that reason, it can be assumed that rising and falling edges are symmetrical. The main conclusion is that the Gauss function gives a more robust fit than the widely used gamma-variate function when modelling concentration-time curves in lung pCT studies.

1 INTRODUCTION

Perfusion computed tomography (pCT) is one of the methods that enable non-invasive imaging of the hemodynamics of organs and tissues. On the basis of pCT measurements, perfusion parameters such as blood flow (*BF*), blood volume (*BV*), mean transit time (*MTT*) and permeability surface (*PS*) are calculated and then used for quantitative evaluation of the tissue condition. Usefulness of perfusion parameters has been proved in the diagnosis of brain (Wintermark et al., 2008), kidneys (Zhao et al., 2010), liver (Mírka et al., 2010), pancreas (Balthazar, 2011) and spleen (Sauter et al., 2012). In the case of lungs, as in other organs, perfusion imaging is particularly useful for diagnosing cancer (Cao, 2011). The method allows not only for establishing the tumour size and location (Nakano et al., 2013), but may also provide important predictive information concerning tumour vasculature (Ng and Goh, 2010). Lung pCT measurements can also help in the diagnosis of diabetic pulmonary microangiopathy (Browarczyk et al., 2015; Kalicka et al., 2015).

The pCT chest technique uses the intravenous injection of a non-iodinated contrast agent (tracer) and the sequential scanning of the chest when the agent passes through the lungs for the first time ("first-pass"). The tissue concentration-time curve $c(t)$ is obtained for every pixel of the diagnosed cross-section. The relationship between the arterial input function tracer concentration $c_{AIF}(t)$ on entering the region of interest (ROI) and the $c(t)$ measured within the ROI has been formulated on the basis of the tracer kinetics theory.

To calculate perfusion parameters it is necessary to approximate the data in the form of $c(t)$ and $c_{AIF}(t)$ measurements with regression function. The most commonly used functions for this purpose are the gamma-variate (Blomley and Dawson, 1997; Jackson, 2004) and two- or three-exponential functions (Kalicka and Pietrenko-Dąbrowska, 2007; Srikanchana et al., 2004). However, regression functions that have good properties when applied to dynamic brain research (Kalicka and Pietrenko-Dąbrowska, 2007) or carotid artery (Lampaskis et al., 2009), demonstrate worse performance, for instance, in the case of renal studies (Balvay et al.,

2008) or liver (Lampaskis et al., 2009). This observation inspired us to compare the gamma-variate function with the Gauss and the Rayleigh functions in pCT lung studies. The Gauss and the Rayleigh functions were not previously used for this purpose. All of the functions were compared using both actual and simulated pCT data.

2 MATERIAL AND METHODS

The clinical measurements were performed on a 64-row Light Speed VCT CT scanner produced by GE Healthcare USA. Pulmonary perfusion was axially evaluated in three cross-sections: the upper, the middle and the lower parts of the lungs (2 cm, 3.5 cm and 5 cm below carina, respectively, see figure 1), 12 s after the intravenous administration of 40 ml a non-iodinated contrast medium at a rate of 4 ml/s. Each of the three sequences consists of 89 scans, with a resolution of 512 at 512 pixels, collected with a sampling interval of 1 s.
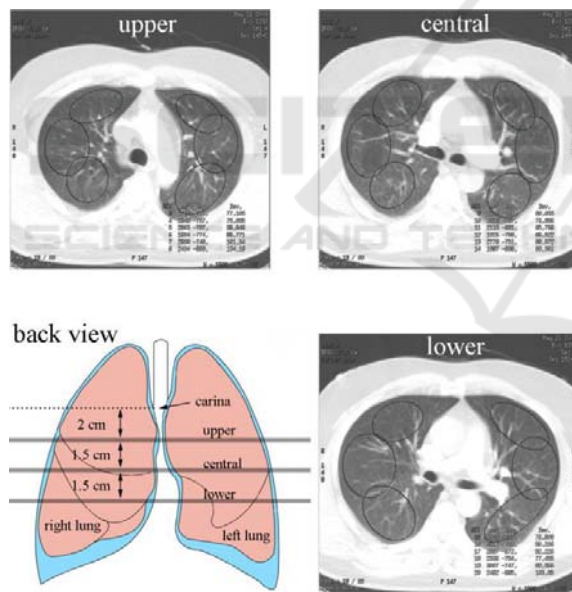

Figure 1: Three cross-sections obtained from healthy subject.

Two data sets were collected. The first data set consists of actual measurements and the second data set was simulated. Simulated data were used for extended analysis of error propagation for all considered regression functions. Each data set, both measured and simulated, consists of three concentration-time curves, one per lung region: arterial input function (AIF), blood vessels and parenchyma. The first data set was created from the actual measurements obtained from 5 healthy subjects, 2 females and 3 males, aged 33-67. The second data set was simulated using the actual measurements obtained from another healthy subject (female, 67 y/o, non-smoking with no diagnosed acute or chronic diseases affecting pulmonary functions). All patients received written information about the study, then gave written consent to participate. The study was approved by the Independent Commission on Bioethics Committee for Scientific Research at the Medical University of Gdańsk.

The simulations were conducted in the following way: 100 pixels were manually chosen from the upper, the central and the lower cross-sections. The selected pixels provide $j=1,...,100$ concentration-time curves $c_j(t_i)$. Each curve consists $i=1,...,89$ measurements. The most typical concentration-time curve $c_{typ}(t_i)$ was calculated as a mean vector, defined as sum of vectors $c_j(t_i)$ divided by number of vectors. The typical curves were used to perform 100 simulation runs $c_{sim}(t_i)$:

$$c_{sim}(t_i) = G\big(c_{typ}(t_i), \mathbf{R}\big) \qquad (1)$$

$G(c_{typ}(t_i),\mathbf{R})$ is the random numbers generator of the normal distribution with mean parameter $c_{typ}(t_i)$ and standard deviation $\mathbf{R}$ equal to the residual variance of actual measurements:

$$\mathbf{R} = \sqrt{\frac{\sum_1^j \big(c_{typ}(t_i) - c_j(t_i)\big)^2}{j(j-1)}}, \; j=100 \qquad (2)$$

Figure 2 shows the $c_{typ}(t_i)$ and an example of a $c_{sim}(t_i)$ for AIF, vessels and parenchyma.

The peaks and valleys (figure 2) are characteristic for pCT lung results. They are caused by the patient's breathing during the examination. In further analysis we consider the peaks which correspond to the phase of inspiration. The peaks were detected using the function *findpeaks* (Mathworks Matlab R2010a). Only the first passage of tracer was modelled.

The following functions were chosen to be compared:

- gamma-variate function;

$$V(v_1, v_2, v_3, t_0, t) = v_1 \cdot (t - t_0)^{v_2} \cdot e^{-\frac{t-t_0}{v_3}} \qquad (3)$$

- Gauss function;

$$G(g_1, g_2, g_3, t) = g_1 \cdot e^{-\frac{(t-g_2)^2}{g_3}} \qquad (4)$$

- Rayleigh;

135

$$R(r_1, r_2, t_0, t) = r_1 \cdot \frac{t - t_0}{r_2^2} \cdot e^{-\frac{(t-t_0)^2}{2 \cdot r_2^2}} \qquad (5)$$

where v_1, v_2, v_3, g_1, g_2, g_3, r_1, r_2 are regression function parameters; t_0 is arrival time of contrast agent, determined empirically.

The values of model parameters $\mathbf{v} = [v_1, v_2, v_3]$, $\mathbf{g} = [g_1, g_2, g_3]$ and $\mathbf{r} = [r_1, r_2]$ were calculated according to the objective function:

$$OF = \frac{1}{N} \sum_{i=0}^{N-1} (c(t_i) - c_{mod}(\mathbf{p}, t_i))^2 = \min$$
$$\mathbf{p} = [p_1, p_2, .., p_{n_p}] = \arg \min OF \qquad (6)$$

where N is number of time points, $\mathbf{p}$ is the parameter vector equal to $\mathbf{v}$, $\mathbf{g}$ and $\mathbf{r}$ for the gamma-variate, the Gauss and the Rayleigh model functions $c_{mod}(t_i, \mathbf{p})$, respectively.

The BV parameter is the relative blood volume in the considered ROI. It is defined as follows (Calamante et al., 1999):

$$BV = \frac{k_H}{\rho} \cdot \frac{\int_0^\infty c(t) dt}{\int_0^\infty c_{AIF}(t) dt} \qquad (7)$$

where k_H is the correction factor accounting for the differences in the hematocrit of capillaries and large vessels, ρ is the tissue density [g/cm3], and $c(t)$ and $c_{AIF}(t)$ are the concentration of contrast agent in ROI and in AIF, respectively. In literature the values of k_H and ρ differ significantly (Chan and Siochi, 2011; Cohen, 1966; Hopkins et al., 2007; Lilienfeld et al., 1956; Pevsner et al., 2005; Praveenkumar et al., 2011). In our research the precise values of k_H and ρ are not relevant. We assume $k_H/\rho = 1$ for all the considered types of tissue: AIF, vessels, parenchyma.

Next, the models will be used to calculate the blood volume BV defined by the equation 7, which is the diagnostically important descriptor of lung perfusion. Errors associated with measurements propagate to the errors associated with model parameters and in turn they propagate to errors of perfusion parameter BV. The way of propagation depends on the particular form of the regression function. We will test different regression functions to compare their built-in, inner potential to provide accurate identification results. To get the aim we will apply methodology and criteria of the error propagation and of the sensitivity analysis.
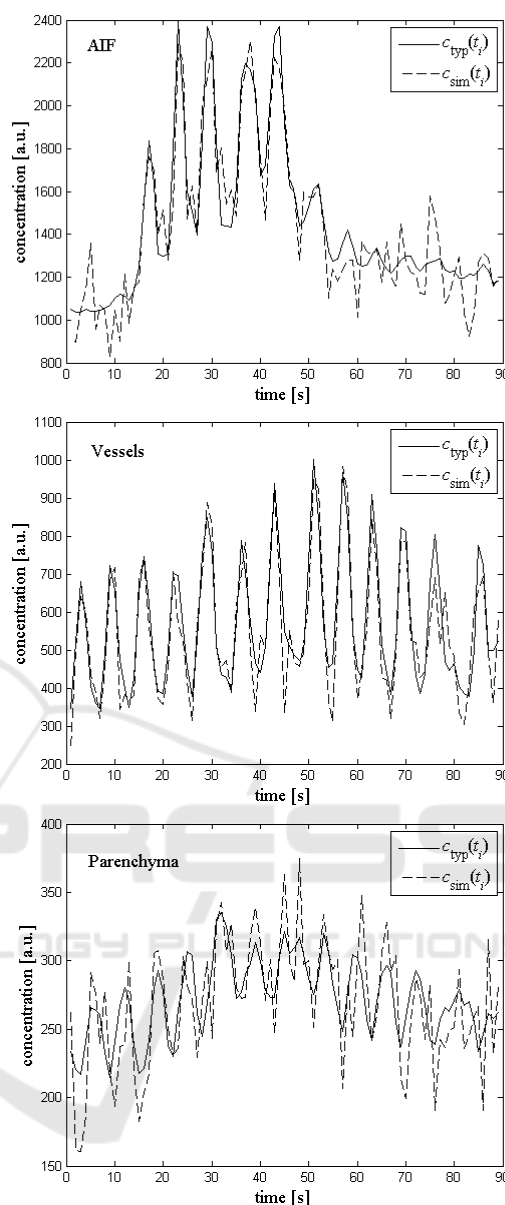
There are two basic questions relating to the

Figure 2: Typical concentration-time curves $c_{typ}(t_i)$ and an example of the simulated curve $c_{sim}(t_i)$ for AIF (upper), vessels (middle) and parenchyma (lower).

identification of model parameters. Is the model identifiable, i.e. whether there is a unique solution in form of model parameters? Whether the parameters can be designated on the basis of the measurements with a satisfactory accuracy?

It is important to obtain unique estimates of all model parameters. This problem is considered as theoretical or a priori identifiability. Sometime a model is theoretically identifiable, but process of parameters estimation may produce such large errors that occurs a loss of practical or a posteriori

identifiability.

Process of parameters estimation requires finding minimum of objective function OF in the parameter space. Dimension of the parameter space is equal to the number of model parameters $n_p \leq N$, N is number of measurements:

$$OF = \frac{1}{N} \sum_{i=0}^{N-1} (y_{meas}(t_i) - y_{mod}(\mathbf{p}, t_i))^2 = \min$$
$$\mathbf{p} = [p_1, p_2, .., p_{n_p}] = \arg \min OF \quad (8)$$

where $y_{meas}(t_i)$ is a set of measurements collected in N time points t_i and $y_{mod}(\mathbf{p}, t_i)$ is a model function that depend on parameter vector $\mathbf{p}$.

Let us analyse sensitivity S_p of $OF(\mathbf{p})$ with respect to estimated parameters – for large and for small sensitivity value. Assume that the resolution of the OF measurement is OF, see Figure 3.
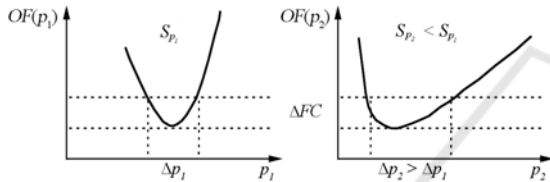

Figure 3: Dependence between the shape of OF and the attainable accuracy for Δp_1 and $\Delta p_2 > \Delta p_1$ for two model parameters p_1 and p_2 and for the same measurement resolution OF.

The larger sensitivity S_p the smaller error p. Therefore, for the same measurement resolution OF, the attainable accuracy p differs depending on the particular sensitivity function. The sensitivities are dependent on the properties of the regression function. Choice of the regression function of desired properties is the aim of our investigation.

The relationship between sensitivity and error one can present in an analytical form:

$$OF = (\mathbf{y}_{meas}(t_i) - \mathbf{y}_{mod}(\mathbf{p}, t_i))^T \cdot (\mathbf{y}_{meas}(t_i) - \mathbf{y}_{mod}(\mathbf{p}, t_i)) \quad (9)$$

where $i = 1, ..., N$ and $\mathbf{p} = [p_1, p_2, ..., p_{np}]$. Differentiating OF with respect to the parameter vector we obtain:

$$\frac{\partial OF}{\partial \mathbf{p}} = -2 \cdot (\mathbf{y}_{meas}(t_i) - \mathbf{y}_{mod}(\mathbf{p}, t_i))^T \cdot \frac{\partial \mathbf{y}_{mod}}{\partial \mathbf{p}}$$

$$\frac{\partial \mathbf{y}_{mod}}{\partial \mathbf{p}} = \mathbf{S} = \begin{bmatrix} \frac{\partial \mathbf{y}_{mod}(\mathbf{p}, t_1)}{\partial p_1} & \frac{\partial \mathbf{y}_{mod}(\mathbf{p}, t_1)}{\partial p_{n_p}} \\ \frac{\partial \mathbf{y}_{mod}(\mathbf{p}, t_N)}{\partial p_1} & \frac{\partial \mathbf{y}_{mod}(\mathbf{p}, t_N)}{\partial p_{n_p}} \end{bmatrix}_{N x n_p} \quad (10)$$

$\mathbf{S}$ is the sensitivity matrix. Searching for error of

parameter estimates involves the searching for variance-covariance matrix of the estimates. Under simplifying assumptions ($y_{mod}(\mathbf{p}, t_i)$ is approximated to a linear factor of Taylor series, the disturbances are uncorrelated, the expected value of the disturbances is zero, and covariance is constant and equal to σ^2) the variance-covariance matrix $\mathbf{P}$ in the vicinity of the minimum of OF, takes the form of (Cobelli et al., 2002; Enderle et al., 2000; Semmelow, 2005):

$$\mathbf{P} = \mathbf{P}_{n_p x n_p} = \sigma^2 (\mathbf{S}^T \mathbf{S})^{-1} \Big|_{\mathbf{p} = \mathbf{p}_{opt}} \quad (11)$$
$$\mathbf{p}_{opt} = \arg(OF(\mathbf{p}) = \min)$$

The matrix $\mathbf{P}$ is symmetric, as the variances are pair wise symmetric. The sensitivity matrix $\mathbf{S}$ elements are the sensitivities of the model output to changes in particular parameters. The entries of the matrix $\mathbf{P}$ are:

$$\mathbf{P}_{n_p x n_p} = \sigma^2 (\mathbf{S}^T \mathbf{S})^{-1} = \sigma^2 \frac{adj(\mathbf{S}^T \mathbf{S})}{\det(\mathbf{S}^T \mathbf{S})} \Big|_{\det(\mathbf{S}^T \mathbf{S}) \to 0} \quad (12)$$

When the matrix becomes singular: $det(\mathbf{S}^T \mathbf{S}) \to 0$, their entries are large and, therefore, associated error estimates are large.

Even if structural identifiability of the model has been previously confirmed, it may happen that the matrix $\mathbf{S}^T \mathbf{S}$ is close to singular. Inversing such matrix $\mathbf{S}^T \mathbf{S}$ cause very large entries of the matrix $\mathbf{P}$, which means a very large errors of parameter estimates. Thus, the matrix $\mathbf{S}^T \mathbf{S}$ must be non-singular and the sensitivity $\mathbf{S}$ large. Both, the sensitivity $\mathbf{S}$ and the matrix $\mathbf{S}^T \mathbf{S}$ depend on the form of regression function y_{mod}. Choice of the regression function of desired properties (large $\mathbf{S}$ and not singular, or not close to singular, the matrix $\mathbf{S}^T \mathbf{S}$) is the aim of our investigation.

We assumed that model function is better than the others if it gives lower objective function OF and lower uncertainty ΔBV values. The smaller value of OF, the better the function fit. According to the error propagation rule, the smaller error p_i of regression function parameters the smaller ΔBV uncertainty of BV. For example, when regression function depends on two parameters p_1 and p_2, then the uncertainty ΔBV is defined as follows (Ku, 1966):

$$\Delta BV = \sqrt{\left(\frac{\partial BV}{\partial p_1}\right)^2 \Delta p_1^2 + \left(\frac{\partial BV}{\partial p_2}\right)^2 \Delta p_2^2 + \left(\frac{\partial BV}{\partial p_1}\right)\left(\frac{\partial BV}{\partial p_2}\right) \Delta^2 p_1 p_2} \quad (13)$$

where Δp_1, Δp_2 are parameters p_1 and p_2 estimation errors, $\Delta p_1 p_2$ is estimated covariance of p_1 and p_2.

In literature it is presented opinion that the first passage of tracer is asymmetrical, i.e. the rising and

falling edges are not equally sloped (Lampaskis et al., 2009; Thompson et al., 1964). In order to examine symmetry between rising and falling edge of concentration-time measurements in pCT lung study, the edges were approximated by linear function in the range of linear edge course. The slope angles φ_R and φ_F were calculated. The asymmetry coefficient ζ was defined as follows:

$$\zeta = \frac{|\varphi_R| - |\varphi_F|}{|\varphi_R|} \cdot 100\% \qquad (14)$$

3 RESULTS

To compare the different regression functions 100 simulation runs were performed. For each simulation run the value of objective function *OF* was calculated for all compared regression functions. Then, for each regression function the mean value of the objective function was calculated. The results obtained for AIF, vessels and parenchyma are presented in table 1 - different regression functions show different ability to fit measurements. Table 2 presents the mean *BV* and *BV* calculated according to the error propagation rule, with respect to all model parameters, for simulated data.

The value of *BV*, for AIF region and for all regression functions, is known a priori and equal to 100, see table 2 and 4. It results from the equation 7: the integrals in numerator and denominator of are equal, so their quotient is equal to 1 and $k_H/\rho = 1$. In literature the *BV* is given in [ml/100g] therefore equation 7 is multiplied by 100.

Table 1: Mean values of objective function for gamma-variate, Gauss and Rayleigh functions in all regions calculated for simulated data.

	gamma-variate	Gauss	Rayleigh
AIF	9258	9198	9201
vessels	808	680	1218
parenchyma	193	186	230

Table 3 shows mean *OF* calculated for the actual measurements taken from 5 subjects. Table 4 shows example results of *BV* and ΔBV for a certain patient calculated based on actual data.

Tables 5 shows rising and falling edge slope angles φ_R and φ_F, their differences and asymmetry coefficients ζ, separately for each of 5 subjects. Table 6 shows mean values of rising and falling edge slope angles φ_R and φ_F, their standard deviations $\Delta\varphi_R$ and $\Delta\varphi_F$, differences between mean

values of φ_R and φ_F and asymmetry coefficients ζ.

Table 2: Mean *BV* parameters; their uncertainties $\pm\Delta BV$ and CV calculated for simulated data, taking into account errors p_i of regression functions parameters p_i.

	BV [ml/100g] $\pm\Delta BV$ [ml/100g] CV [%]		
	gamma-variate	Gauss	Rayleigh
AIF	100 ±0,2626 0,2626	100 ±0,0760 0,0760	100 ±0,2447 0,2447
vessels	19,1400 ±61,5489 321,5700	19,9783 ±0,0058 0,0290	21,0502 ±0,0333 0,1582
parenchyma	6,1652 ±0,0680 1,1030	6,2627 ±0,0004 0,0064	5,6497 ±0,0051 0,0903

Table 3: Mean values of objective function for gamma-variate, Gauss and Rayleigh functions in all regions calculated for 5 subjects, based on actual data.

	gamma-variate	Gauss	Rayleigh
AIF	9411	7791	9129
vessels	853	706	1401
paren.	136	130	139

Table 4: Example results of *BV* parameter; its uncertainty $\pm\Delta BV$ and CV calculated for single subject (female, 63 years old), taking into account errors p_i of regression functions parameters p_i, based on actual data.

	BV [ml/100g] $\pm\Delta BV$ [ml/100g] CV [%]		
	gamma-variate	Gauss	Rayleigh
AIF	100 ±0,1170 0,1170	100 ±0,0311 0,0311	100 ±0,2505 0,2505
vessels	10,3512 ±20,2722 195,8440	8,5467 ±0,0037 0,0433	11,0668 ±0,0158 0,1428
parenchyma	8,4072 ±0,0084 0,0999	8,1724 ±0,0004 0,0049	8,3620 ±0,0075 0,0897

Table 5: Rising and falling edge slope angles φ_R and φ_F, their differences and asymmetry coefficients ζ calculated for 5 subjects, based on actual data.

		φR [°]	φF [°]	|φR|-|φF| [°]	ζ [%]
	AIF	88,24	-88,70	-0,46	-0,52
1	vessels	87,26	-86,04	1,22	1,40
	parenchyma	77,64	-75,41	2,23	2,87
	AIF	86,71	-87,94	-1,23	-1,42
2	vessels	85,53	-84,56	0,97	1,13
	parenchyma	74,86	-69,65	5,21	6,96

Table 5: Rising and falling edge slope angles φR and φF, their differences and asymmetry coefficients ζ calculated for 5 subjects, based on actual data (cont.).

	AIF	89,59	-89,02	0,57	0,64
3	vessels	85,37	-87,16	-1,79	-2,10
	parenchyma	71,83	-73,00	-1,17	-2,57
	AIF	88,41	-88,15	0,26	0,29
4	vessels	84,42	-75,40	9,02	10,69
	parenchyma	79,22	-66,50	12,72	16,06
	AIF	88,91	-88,96	-0,05	-0,06
5	vessels	86,40	-86,30	0,10	0,12
	parenchyma	64,73	-66,50	-1,77	-2,73

Table 6: Mean values of rising and falling edge slope angles φR and φF, their standard deviations φR and φF, differences and asymmetry coefficients ζ calculated for 5 subjects, based on actual data.

	φR [°] ±ΔφR [°]	φF [°] ±ΔφF[°]	|φR|- |φF| [°]	ζ [%]
AIF	88,37 ±1,07	-88,55 ±0,49	-0,18	- 0,21
vessels	85,80 ±1,08	-83,89 ±4,84	1,90	2,22
parenchyma	73,66 ±5,73	-70,21 ±3,96	3,44	4,68

4 DISCUSSION

Our aim is to determine which function best approximates the first passage of tracer in pCT lung studies. Fitting results, presented in table 1, show different quality of fit for different regression functions. Taking into account *OF* values, the Gauss function proved to be the best in all considered regions - AIF, vessels and parenchyma. Similar conclusions can be drawn on the basis of uncertainty analysis, see table 2. It is worth mentioning, that the most frequently used gamma-variate function produced noticeably higher *BV* than the Gauss and the Rayleigh functions.

Simulated data analysis demonstrated the advantage of the Gauss function over the other ones. In order to confirm the simulation results, actual measurements analysis was performed. The results, presented in table 3, show that *OF* in all regions are the lowest for the Gauss function. The Gauss function best approximates the first passage of tracer in AIF, blood vessels and parenchyma. Also, the Gauss function produces the lowest uncertainty *BV*, which means that the impact of model parameters error on *BV* is the smallest.

It is widely accepted that the first passage of tracer is asymmetrical, i.e. the rising and falling edges are not equally sloped (Lampaskis et al., 2009; Thompson et al., 1964). Considering this, regression function that best approximates the first passage of tracer should also be asymmetrical. However, it was proved (table 1 and table 3) that the Gauss function, which is symmetrical, best approximates the first passage of tracer. The rising and falling edges of concentration-time curves were approximated by the linear function and slope angles were calculated. Rising and falling edge slope angles, their differences and asymmetry coefficients calculated for 5 subjects are presented in table 5. Furthermore, the mean values of slope angles, their standard deviations, differences and asymmetry coefficients were calculated and presented in table 6. Differences between slope angles are insignificant and the differences between mean values of rising and falling edge slope angles, presented in table 6, are negligible. Therefore, it can be assumed that rising and falling edges of actual measurements are symmetrical (very close to symmetrical). For that reason, the Gauss function proved to be best approximation of the first passage of tracer in pCT lung studies.

5 CONCLUSIONS

This paper presents a comparative analysis of three regression functions in three regions (AIF, blood vessels and parenchyma) in pCT lung tests. Considering results of simulated data analysis, the Gauss function showed a clear advantage over the others. Results of actual measurements analysis confirmed that the Gauss function produce the most accurate approximations of the first passage of tracer. It was showed that contrary to the widely accepted practice, the differences between rising and falling edge slope angles of concentration-time curves are inconsiderable. Therefore, one can assume that rising and falling edges are symmetrical. Negligible asymmetry of measurements justifies why the Gauss function best approximates the first passage of tracer in pCT lung studies.

ACKNOWLEDGEMENTS

REFERENCES

Balthazar, E. (2011). CT Contrast Enhancement of the Pancreas: Patterns of Enhancement, Pitfalls and Clinical Implications. *Pancreatology*, 11(6), pp.585-587.

Balvay, D., Ponvianne, Y., Claudon, M. and Cuenod, C. (2008). Arterial input function: Relevance of eleven analytical models in DCE-MRI studies. In: *Proceedings of 5th IEEE International Symposium on Biomedical Imaging*. Paris: IEEE.

Blomley, M. and Dawson, P. (1997). Bolus dynamics: theoretical and experimental aspects. *The British Journal of Radiology*, 70(832), pp.351-359.

Browarczyk, M., Kalicka, R. and Lipiński, S. (2015). Lung Perfusion Parameters in the Diagnosis of Diabetic Pulmonary Microangiopathy. In: I. Lacković and D. Vasic, ed., *6th European Conference of the International Federation for Medical and Biological Engineering*, 1st ed. Dubrovnik: Springer International Publishing, pp.444-447.

Calamante, F., Thomas, D., Pell, G., Wiersma, J. and Turner, R. (1999). Measuring Cerebral Blood Flow Using Magnetic Resonance Imaging Techniques. *Journal of Cerebral Blood Flow & Metabolism*, pp.701-735.

Cao, Y. (2011). The Promise of Dynamic Contrast-Enhanced Imaging in Radiation Therapy. *Seminars in Radiation Oncology*, 21(2), pp.147-156.

Chen, M. and Siochi, R. (2011). Feasibility of using respiratory correlated mega voltage cone beam computed tomography to measure tumor motion. *Journal of Applied Clinical Medical Physics*, 12(2), p.3473.

Cobelli, C., Foster, D. and Toffolo, G. (2002). *Tracer kinetics in biomedical research*. New York: Kluwer Academic.

Cohen, M. (1966). The Organization of Clinical Dosimetry: I. the four stages of clinical dosimetry. *Acta Radiologica: Therapy, Physics, Biology*, 4(3), pp.233-256.

Enderle, J., Blanchard, S. and Bronzino, J. (2000). *Introduction to biomedical engineering*. San Diego: Academic Press.

Hopkins, S., Henderson, A., Levin, D., Yamada, K., Arai, T., Buxton, R. and Prisk, G. (2007). Vertical gradients in regional lung density and perfusion in the supine human lung: the Slinky effect. *Journal of Applied Physiology*, 103(1), pp.240-248.

Jackson, A. (2004). Analysis of dynamic contrast enhanced MRI. *The British Journal of Radiology*, 77(suppl_2), pp.S154-S166.

Kalicka, R. and Pietrenko-Dąbrowska, A. (2006). Parametric Modeling of DSC-MRI Data with Stochastic Filtration and Optimal Input Design Versus Non-Parametric Modeling. *Annals of Biomedical Engineering*, 35(3), pp.453-464.

Kalicka, R., Browarczyk, M. and Lipiński, S. (2015). Usefulness of chest perfusion computed tomography in the diagnosis of diabetic pulmonary microangiopathy. *Biocybernetics and Biomedical Engineering*, 35(1), pp.68-73.

Ku, H. (1966). Notes on the use of propagation of error formulas. *Journal of Research of the National Bureau of Standards, Section C: Engineering and Instrumentation*, 70C(4), p.263.

Lampaskis, M., Strouthos, C. and Averkiou, M. (2009). Application of tracer dilution models for the quantification of perfusion with contrast enhanced ultrasound imaging. In: *Proceedings of 14th European Symposium on Ultrasound Contrast Imaging*. Rotterdam.

Lilienfield, L., Kovach, R., Marks, P., Hershenson, L., Rodnan, G., Ebaugh, F. and Freis, E. (1956). THE HEMATOCRIT OF THE LESSER CIRCULATION IN MAN 12. *Journal of Clinical Investigation*, 35(12), pp.1385-1392.

Mírka, H., Ferda, J., Baxa, J., Třeška, V., Liška, V., Schmidt, B. and Flohr, T. (2010). Perfusion CT of the liver. *Czech Radiology*, 64(4), pp.281-289.

Nakano, S., Gibo, J., Fukushima, Y., Kaira, K., Sunaga, N., Taketomi-Takahashi, A., Tsushima, Y. and Mori, M. (2013). Perfusion Evaluation of Lung Cancer. *Journal of Thoracic Imaging*, 28(4), pp.253-262.

Ng, Q. and Goh, V. (2010). Angiogenesis in Non-small Cell Lung Cancer. *Journal of Thoracic Imaging*, 25(2), pp.142-150.

Pevsner, A., Nehmeh, S., Humm, J., Mageras, G. and Erdi, Y. (2005). Effect of motion on tracer activity determination in CT attenuation corrected PET images: A lung phantom study. *Med. Phys.*, 32(7), p.2358.

Praveenkumar, R., Augustine, A. and Santhosh, K. (2011). Estimation of inhomogenity correction factors for a Co-60 beam using Monte Carlo simulation. *Journal of Cancer Research and Therapeutics*, 7(3), p.308.

Sauter, A., Feldmann, S., Spira, D., Schulze, M., Klotz, E., Vogel, W., Claussen, C. and Horger, M. (2012). Assessment of Splenic Perfusion in Patients with Malignant Hematologic Diseases and Spleen Involvement, Liver Cirrhosis and Controls Using Volume Perfusion CT (VPCT). *Academic Radiology*, 19(5), pp.579-587.

Semmlow, J. (2005). *Circuits, signals, and systems for bioengineers*. Oxford: Academic.

Srikanchana, R., Thomasson, D., Choyke, P. and Dwyer, A. (2004). A comparison of pharmacokinetic models of dynamic contrast enhanced MRI. In: *Proc. IEEE Symp. Computer-Based Med. Syst.*. Bethesda: IEEE, pp.361-366.

Thompson, H., Starmer, C., Whalen, R. and Mcintosh, H. (1964). Indicator Transit Time Considered as a Gamma Variate. *Circulation Research*, 14(6), pp.502-515.

Wintermark, M., Sincic, R., Sridhar, D. and Chien, J. (2008). Cerebral perfusion CT: Technique and clinical applications. *Journal of Neuroradiology*, 35(5), pp.253-260.

Zhao, H., Gong, J., Wang, Y., Zhang, Z. and Qin, P. (2010). Renal hemodynamic changes with aging: a preliminary study using CT perfusion in the healthy elderly. *Clinical Imaging*, 34(4), pp.247-250.